Atmos. Chem. Phys. Discuss., 15, 3285–3325, 2015
www.atmos-chem-phys-discuss.net/15/3285/2015/
doi:10.5194/acpd-15-3285-2015

Atmospheric Chemistry and Physics Discussions

Impacts of atmospheric circulations on aerosol distributions in autumn over eastern China: observational evidences

X.-Y. Zheng[1], Y.-F. Fu[1,2,3], Y.-J. Yang[1,3], and G.-S. Liu[1,4]

[1]School of Earth and Space Sciences, University of Science and Technology of China, Hefei, 230026, China
[2]State Key Laboratory of Severe Weather, Chinese Academy of Meteorological Sciences, Beijing, 100081, China
[3]Key Laboratory of Atmospheric Sciences and Satellite Remote Sensing of Anhui Province, Anhui Institute of Meteorological Sciences, Hefei, 230031, China
[4]Department of Meteorology, Florida State University, Tallahassee, 32306–4520, USA

Received: 18 November 2014 – Accepted: 13 January 2015 – Published: 5 February 2015

Correspondence to: Y.-F. Fu (fyf@ustc.edu.cn)

Published by Copernicus Publications on behalf of the European Geosciences Union.

Abstract

Regional heavy pollution events in East China (110–122° E, 28–40° N) are the main environmental problems recently because of the high urbanization and rapid economic development connected with too much emissions of pollutants. However, appropriate weather condition is another factor which cannot be ignored for these events. In this study, the relationship between regional pollution status and larger scale atmospheric circulations over East China in October is investigated using ten-year (2001–2010) MODIS/Terra aerosol optical depth (AOD) product and the NCEP reanalysis data together with case analysis and composite analysis. Generally, statistics in East China show values of mean AOD vary from 0.3 to 0.9 in October over the region, and larger AOD variances are accompanied with the distribution of higher average AOD. Eighteen pollution episodes (regional mean AOD > 0.6) and ten clean episodes (regional mean AOD < 0.4) are selected and then categorized into six polluted types and three clean types, respectively. Each type represents different weather pattern associated with the combination of lower and upper atmospheric circulation. Generally, the uniform surface pressure field in East China or steady straight westerly in middle troposphere, particularly the rear of anticyclone at 850 hPa, are typical weather patterns responsible for heavy pollution events, while clean episodes occur when strong southeastward cold air advection prevails below the middle troposphere or air masses are transported from sea to the mainland. The above studies are especially useful to the government decision make on balance of economic activities and pollution mitigations.

1 Introduction

Concerning that aerosols can perturb the radiation budget of the Earth–atmosphere system, influence the climate, and degrade air quality (Kaufman et al., 2002), they have attracted high attention for a long time (Twomey, 1977; Rosenfeld et al., 2004; Zhao et al., 2006a, b, 2012, 2013a, b; Rosenfeld et al., 2007; Li et al., 2011; Ko-

ACPD
15, 3285–3325, 2015

ren et al., 2012; Chen et al., 2014). Particularly, with the rapid urban growth and development of various industries during last decades, the high concentration of atmospheric pollutants has become one of the major environmental problems which usually pose threats to human health (Donaldson et al., 2001; Kan and Chen, 2004; Janssen et al., 2011). However, appropriate weather condition is another factor which cannot be ignored for these environmental problems (Zhao et al., 2010; Xu et al., 2011). Therefore, to understand the mechanisms that control spatiotemporal distribution of aerosols, extensive investigations have been carried out to study the relationship between the air quality and multiple factors Generally, although the characteristics of regional air quality over a region depend on many complex elements, the major contributions are the emission of the pollutants together with large scale meteorological conditions (X. L. Chen et al., 2008; Z. H. Chen et al., 2008). Ziomas et al. (1995) pointed out that in an urban environment, the serious air pollution episodes are not attributed to sudden increases in the emissions of pollutants but caused by meteorological conditions which are unfavorable for dispersion. Normally, the anthropogenic emissions of widespread pollutant sources are quasi-stable in East China, air pollution status here is subject to large scale atmospheric conditions to a great extent (Xu et al., 2011). In some other regions, strong links between the concentrations of aerosols and certain synoptic weather conditions have already been identified (Demuzere et al., 2009; Saavedra et al., 2012). It has also been revealed that under the circumstances of the same pollutant emission quantity, the ground concentrations of pollutants vary directly with different synoptic patterns (Wang et al., 2001).

In fact, the weather condition which consists of a number of meteorological parameters (wind speed and direction, temperature, relative humidity, precipitation etc.) and synoptic patterns analyzed in terms of atmospheric circulations, can contribute to the vertical redistribution and long-range transport of air pollutants leading to an accumulation or a dispersion of aerosols (Cheng et al., 2007; Ding et al., 2009). A growing body of research is showing the important effects of weather conditions on distribution of pollutants and atmospheric pollution levels. For example, Tanner and Law (2002)

ACPD
15, 3285–3325, 2015

investigated the impacts of meteorological parameters (wind speed, wind direction, temperature, relative humidity and solar radiation intensity) on the frequency of high-level pollution episodes in Hong Kong. Ding et al. (2004) successfully simulated the wind patterns of sea–land breezes and the planetary boundary layer (PBL) heights to illustrate the meteorological cause of the photochemical ozone episode, which is associated with Typhoon Nari, in the Pearl River Delta of China. They contrast the characteristics of dispersion and transport on pre-episode and episode days. Xu et al. (2011) confirmed the deterministic impacts of wind speed and wind direction on the concentration of various trace gases at Wuqing, a suburban site between 2 mega-cities. Csavina et al. (2014) examined dust events in two semi-arid sites, and then showed a complex, nonlinear dependence of PM_{10} on wind speed and relative humidity.

Since meteorological parameters is taken under control of atmospheric circulation (Liu and Li, 1980; Kassomenos et al., 2003), consequently, instead of using different kinds of weather factors, some relevant studies that used atmospheric circulation patterns have been carried out. For example, Shahgedanova (1998) employed components analysis and cluster analysis for Moscow to develop seasonal synoptic indices which can examine weather-induced variability in CO and NO_2 concentrations, they concluded that anticyclonic conditions in spring, summer and autumn are introductive to high pollution levels. Flocas et al. (2008) assessed the circulation patterns at the mean sea level for a period of 15 years and distinguished four synoptic scale types, they found the presence of an anticyclone accounted for highest percentage of pollution episode over Greece. Moreover, Zhang et al. (2010) used numerical mode method to simulate the impacts of weak/strong monsoon circulations on interannual variations of aerosols over eastern China under the conditions of same anthropogenic emissions, they suggested that the decadal-scale weakening of the East Asian summer monsoon is responsible for the increase in aerosol concentrations over eastern China. By using independent satellite products, Zhao et al. (2010) showed consistent disappearance of CO and O_3 enhancements over southeastern China at the onset of East Asian summer monsoon and reemergence after the monsoon wanes, these confirmed strong

ACPD
15, 3285–3325, 2015

modulation effects of monsoon system on regional air quality. Liu et al. (2013) further demonstrated a potential influence from the variation of large-scale circulation, El Nino Southern Oscillation, upon the interannual fluctuation of summertime aerosol optical depth (AOD). Russo et al. (2014) applied the analysis on 10 basic circulation weather types characterized through the use of a set of indices, and their results showed that easterlies prevailed during pollution episodes of three pollutants (NO_2, PM_{10}, O_3) in Portugal.

The aforementioned works suggest that synoptic types play a crucial role in the formation of a pollution episode, they established predictive connection between air quality and circulation patterns over various regions, and provided valuable scientific basis for weather forecast operation. To the authors' knowledge, even though some attempts have been conducted to study the similar relationships in China, most of them chose a single city (Wang et al., 2007; X. L. Chen et al., 2008; Guo et al., 2013) rather than a regional scale area (e.g., East China in this study) as case studies. East China, as a highly urbanized region, with rapidly increasing of industrial and automotive emissions, is frequently characterized by poor air quality (Ding et al., 2008; He et al., 2012). Therefore, the understanding of a predictable relationship between circulation patterns and air qualities is considered significant for the quick indication of the pollution episodes.

In present study, we evaluated the above relationship during autumn using ten-year (2001–2010) MODIS/Terra aerosol optical depth (AOD) product and atmospheric circulations of NCEP reanalysis data. The choice of autumn is in consideration of the following reasons. First, in contrast with other seasons, the local atmosphere structure of autumn is more stable and mainly influenced by the large-scale synoptic system, the dynamic impact is stronger than the thermal effect. These features reduce the influence of complex mesoscale weather systems and small-scale weather disturbances, thus more suitable for the study of large-scale atmospheric circulations. Second, the wet deposition effect is weaker due to the less precipitation in autumn (Chen et al., 2012), which also ensures the availability of AOD data. Finally, previous researches rarely

ACPD
15, 3285–3325, 2015

focused on the pollution episodes during autumn. The paper is organized as follows: a brief introduction of the data and processing methodology used in this study is presented in Sect. 2. In Sect. 3, we describe the interannual variability of AOD over East China and then extend our exploration to the relationships between AOD and characteristics of synoptic circulations through statistical and synthetic analysis. After that, conclusions are given in Sect. 4, in which general characteristics of various types associated with different spatial distributions of AOD over East China are summarized.

2 Data and methods

Data used in this study and methods for sampling high/low AOD cases are described in this section. The research considers the period from 2001 to 2010 and the region between 110 to 122° E, 28 to 40° N. Since we focus on the season of autumn, October is selected as a representative month for investigation.

2.1 AOD data

The main data set used to describe air quality is the daily averaged Collection 5.1 level 3 AOD products (at 1° horizontal resolution) which are derived from the Terra's Moderate-resolution Imaging Spectroradiometer (MODIS), data products are accessible at http://ladsweb.nascom.nasa.gov/data/search.html. Compared to the ground based data, MODIS provides long-term continuous observations for the spatial and temporal distribution of aerosol, which is convenient for developing multi-aspect researches. AOD is the degree to which aerosols prevent the transmission of light by scattering or absorption effect. By using the MODIS/Terra aerosol data, Kim et al. (2007) evaluated the temporal and spatial variation of aerosols over East Asian. Wu et al. (2013) pointed out that MODIS data were usually valid throughout China and then revealed characteristics of aerosol transport and different extinction features in East Asia. Luo et al. (2013) identified the well performance of MODIS AOD over land

ACPD
15, 3285–3325, 2015

in China and they used 10 years data to construct the climatology of AOD over China. According to previous validations, MODIS AOD data are applicable in Chinese regions and can capture the aerosol distributive characters.

Actually, the AOD data are widely used to enhance the understanding of changes in air quality over local, regional, and global scales as a result of their sensitivity to total abundance of aerosols (Chu et al., 2002; Al-Saadi et al., 2005; Lin et al., 2010). AOD can indicate the air quality to a certain degree, the higher the AOD value is, the worse air quality becomes (Liu et al., 2013). In this study, we discuss the cases of pollution and clean separately.

2.2 Meteorological data

The corresponding atmospheric fields analyses performed in this paper are based on the results of meteorological reanalysis products made available by the National Center for Environmental Prediction (NCEP) and National Center for Atmospheric Research (NCAR). For a complete discussion, we consider both surface and upper-air circulation patterns. Zorita and Storch (1999) revealed that sea level pressure field had a relatively stable correlation with other surface meteorological factors. Besides, the 850 and 500 hPa level are selected as the typical height of lower and middle troposphere, respectively. Mean sea level pressure and surface temperature, geopotential height and temperature at the 500 hPa level, wind field and geopotential height at the 850 hPa level were extracted from NCEP/NCAR Reanalysis dataset on a $2.5^{\circ} \times 2.5^{\circ}$ latitude/longitude grid on a daily basis (http://www.esrl.noaa.gov/psd/data/gridded/data.ncep.reanalysis.html).

2.3 Methods

On the basis of ten-year October data, namely 310 days, we get the daily AOD distribution. According to the threshold of AOD (mentioned in Sect. 3.1), the whole 310 days are divided into four categories: high AOD (> 0.6), low AOD (< 0.4), median AOD

ACPD
15, 3285–3325, 2015

(0.4 ∼ 0.6) and the missing-value day (due to clouds). Ignoring the group of missing and median data, the circulation fields correspond to the other two categories (high AOD and low AOD) are evaluated at the same time. Since satellite-based AOD exists certain uncertainties, therefore, the consecutive days of high (or low) value can better illustrate the existence of the air pollution than just one day. And statistical results of two categories also show that the occurrence of high (or low) value of AOD inclined to last for several days. Besides, the corresponding circulation pattern is also quasi-steady during these high (or low) AOD periods.

Taking the above facts into account, the first synthetic process are conducted by averaging the corresponding grid point values for successive days (greater than or equal to 2 days) presented as high (or low) AOD. Following this approach, 28 episodes, among which there are 18 high-value episodes (HEs) and 10 low-value episodes (LEs), are initially identified during 2001–2010. In order to obtain the statistical characteristics of the pollution and clean episodes, the second synthetic process is performed. We classify the 18 HEs and 10 LEs obtained in the first step on a synoptic basis and average the similar circulations for these two different categories respectively, a thorough description of results obtained by this method can be found in Sect. 3.3. The 18 HEs are clustered into six types while 10LEs are three types. Thus, nine distinct circulation types are consequently considered in the following analyses.

2.4 Hybird Single-Particle Lagrangian Integrated Trajectory (HYSPLIT) model

The backward trajectories for two typical episodes discussed in Sect. 3.2 are simulated using the HYSPLIT model, employing NCEP/NCAR reanalysis meteorological data as input fields. With powerful computational capabilities, the HYSPLIT_4 model is a widely-used system for calculating simple trajectories to complex dispersion and deposition simulations using either puff or particle approach (readers are referred to Draxler and Hess (1997) for more detail of the model). Borge et al. (2007) used back trajectories computed with HYSPLIT model to examine the impact of long-range atmospheric transport on urban PM_{10} for three cities. Chen et al. (2013) incorporated eight

ACPD
15, 3285–3325, 2015

size PM fractions of metals to the HYSPLIT model and provided a prediction of the size distribution and concentrations of heavy metals. In this work, the air-mass trajectories are evaluated in order to present the different movement of air parcels during the two contrary episodes.

3 Results

3.1 Climatological mean and interannual variation

Prior to the analysis of the link between air quality and large-scale circulations, it is necessary to reveal the backgrounds that climatological mean and interannual variation of AOD in October over East China. The climatological mean AOD from MODIS are obtained for the period from 2001 to 2010. As shown in Fig. 1a, the spatial distribution show AOD ranges from 0.3 to 0.9 for almost the entire area. Four prominent centers of high AOD values are found in East China, i.e., Bohai Gulf, Yangtze River delta, junctional areas of Anhui, Shangdong and Henan provinces, and most parts of Hubei and Hunan provinces which were recognized as the source of high emissions in October according to Wang and Zhang (2008). In other words, these centers are considered as possible consequences of industrial emissions or agricultural biomass burning which occurs in autumn with certain meteorological conditions. Figure 1b presents the SD of AOD for the same period. The distribution pattern of Fig. 1b is similar to that of Fig. 1a, which means the SD is larger over the region where the mean AOD is higher. Moreover, the climatological mean wind vectors at 850 hPa and geopotential height are shown in Figs. 1c and d. Obviously, weak counterclockwise winds at 850 hPa (Fig. 1c) and flat western flow at 500 hPa (Fig. 1d) level suggest that East China is dominated by the large-scale stable circulation without the frequent disturbances of small-scale weather systems. Interannually, we show ten-year distribution of AOD anomaly over East China in October (spatial distribution in Fig. 2a and regional mean in in Fig. 2b). Significant annual variations of AOD are found over East China, the maximum deviation is about

ACPD
15, 3285–3325, 2015

0.4, most of the area is less than 0.2. Especially, the 2003 and 2006 represent the most distinct lowest and highest aerosol year, respectively.

In order to depict the frequency of pollution event and give the threshold beyond which the value can be regarded as high AOD, we count the frequency distribution of high AOD (> 0.5 and > 0.6) plotted in Fig. 3. Luo et al. (2014) considered the value of AOD > 0.5 as the high value in China. However, for more than half of East China, it is found that the frequency of AOD > 0.5 is larger than 50 % (Fig. 3a). Consequently, we define 0.6 as the rigor critical value. Compared to Fig. 3a, the area with relative high frequency reduces in Fig. 3b, and the frequency of above 65 % area of East China is less than 50 %. On the contrary, the day is classified into the low-value group on condition that the value of regional mean AOD over the study area is less than 0.4. Furthermore, according to the topography shown in Fig. 3c, it is evident that the emergence of high frequency is related closely to the terrain of East China. It notes that the pattern of high frequency distribution (Fig. 3b) is consistent with that of high values of ten-year mean AOD distribution (Fig. 1a). High AOD mainly concentrated in plain and hilly areas, especially the economically developed Yangtze River Delta, which are characterized by dense population along with a great number of industrial and vehicle emissions.

3.2 Two typical cases: high and low AOD

On the basis of the above results, two typical cases are presented in this section to show the differences between pollution and clean episodes. The process during 28–31 October 2006 is analyzed as a typical high AOD episode (HE) example, whereas the 4 days from 21 to 24 October in 2003 are selected as a typical low value episode (LE).

The mean patterns of AOD and atmospheric circulations at surface, 850 hPa level, 500 hPa level in the period of the HE example are given in Fig. 4. The regional average AOD of HE is 0.76 which signified a pollution process, and maximum value was greater than 1.2. The corresponding sea level pressure pattern (Fig. 4b) were almost controlled by uniform pressure field without obvious control effect, and the shallow

ACPD
15, 3285–3325, 2015

trough promoted west-northwest flow at 500 hPa (Fig. 4d), which represented a stable synoptic pattern and was conductive to the storage of air pollutants. During this period, the main feature of wind filed at 850 hPa level was the weak clockwise circulation centered at Shanxi province, wind blew from the north in East China under the control of a large scale anticyclone (Fig. 4c).

Figure 5 shows the mean patterns of LE example from 21 to 24 October in 2003. Unlike the polluted episodes (Fig. 4a) when the whole East China was masked by high aerosol loadings except a small area in northwest, the area was mainly influenced by low AOD (< 0.4) (Fig. 5a). And the mean AOD (0.38) was at half the level HE reached. In Fig. 5b, the surface circulation of LE showed a uniform field similar to HE, but high-pressure system was relatively weak and the pressure gradient over northern areas was slightly stronger than that of HE. Moreover, compared to the northerly of ~ 1–$4\,m\,s^{-1}$ in HE episode (Fig. 4c), stronger northwesterly winds of ~ 6–$9\,m\,s^{-1}$ were observed at 850 hPa (Fig. 5c). Furthermore, the temperature and geopotential height in the middle troposphere (500 hPa) indicated a strong northwesterly flow prevailed over East China and led cold air masses to low-mid latitude (Fig. 5d). These conditions played an important role in the horizontal diffusion of air pollutants.

In addition, to describe different air mass sources and transport path, HYSPLIT model was applied to the days when the two typical episodes occurred. For each day, we calculated the backward trajectories originated from three locations and the associated ending height is 1000 m above ground level. Trajectories were considered to be initiated at 02:00 (UTC) when MODIS/TERRA passes across China, terminating at the end of 48 h. As shown in Fig. 6, the backward trajectories of four polluted day (Fig. 6a) were composed of short tracks, which were mainly trapped in East China. This indicated that the pollution was caused by the combination of the circulation pattern which gone against dissipation of air pollutants and a great deal of local emissions in the studied area. In contrast, the LE presents a cluster of relatively longer trajectories corresponded to fast-moving air mass from Mongolia. Northwesterly cold winds on these days dispersed local air pollutants, and also brought clean air.

ACPD
15, 3285–3325, 2015

3.3 All selected cases

The aforementioned case studies show that, without considering the variations in emission, some synoptic types are favorable to the occurrence of the air pollution while others are quite contrary. A comprehensive statistic of all cases in the study period over East China is conducted. Excluding all missing and median days, the total 121 days are extracted for the research, of which there are 90 days with high AOD and 31 days with low AOD. Tables 1 and 2 list the statistical results of 18 pollution episodes and 10 clean episodes respectively.

It is found from Table 1 that 2002 and 2006 are both years with maximum occurrence (16 days) of pollution, and this is in accord with the high value presented in Fig. 2. The estimated duration of pollution episodes, on a daily basis, mostly lasts for about four days or longer. To be more specific, for sea level pressure field, the most frequent pattern is characterized as the periphery of the high pressure centered in the Tibetan plateau or Mongolia, amounts to 38 days. The uniform pressure over the East China is the second high-frequency type with a percentage of 37 %, namely 34 days. Among the remaining three types, one is interpreted as the pattern before the passage of a cold front, and the corresponding pattern in lower troposphere (850 hPa) is characterized as strong cold air flow moves toward the East China, which involves 2 episodes (6 days). The other 15 episodes are dominated by the anticyclonic circulation in 850 hPa, it is noted that the region is controlled by the different part of anticyclones, the frequency of the rear of anticyclone is 35 days, while the frequency of the foreside and the center of anticyclone are both 23 days. For patterns of 500 hPa geopotential height, there are 30 days influenced by the northwest (NW) flow, of which 19 days were caused by the upper air trough. The number of days associated with the west-northwest (W-NW) flow and west (W) flow, is 19 and 7, respectively, in addition, the southwest (SW) flow prevailed during a three-day episode.

Table 2 is same as Table 1, but for 10 clean episodes. According to the Table 2, the number of low-value day peak in 2003.The high pressure centered in the northwest of

ACPD
15, 3285–3325, 2015

China on surface is the frequent patterns since it accounts for 15 days of the whole 31 clean days. Besides this, 8 days go through the passage of a cold front and the rear of a high pressure system over the Yellow Sea follows with a frequency of 5 days, the rest 3 days is characterized by the uniform pressure field. For 850 hPa wind fields, frequency of the pattern dominated by anticyclonic wind vectors over the study area is the highest, it is 12 days. Secondly, it is the anterior part of anticyclone (11 days) and the rest two episodes related to the upper air cold front bring strong and cold stream southwardly in the lower troposphere. The 500 hPa geopotential height of clean episodes, unlike that of pollution episodes, include only two dominant airflow directions. For most of clean days, the northwest flow prevails, whereas the other 5 days are associated with the flat west stream.

The characteristics of circulation patterns of all pollution episodes and clean episodes at each level are gained through the above statistics. In terms of a single level (surface/850/500 hPa), the circulation patterns for different episodes are similar. However, it is the combination of circulations at lower level and upper level that the air quality always depends on. The rows in Tables 1 and 2 with same capital letters in the parentheses following the sequence number indicate those episodes are affected by the similar circulation patterns in all the three atmospheric levels. There are nine different letters in two tables, namely, the entire 28 episodes are classified into nine different types, among which there are six pollution types and three clean types.

3.4 Statistics and synthetic analysis

Based on the above results of all cases, nine types are detailedly inspected in this section. Before the description of each type, it is pointed out that the mean AOD and meteorological fields for each type, which consist of the sea level pressure and surface temperature, the 850 hPa wind and geopotential height, the 500 hPa geopotential height and temperature, are averaged from the several episodes that marked with same letter in Table 1 (Table 2). The percentage of each pollution (clean) type is calculated on a daily basis. More specifically, Figs. 7–12 present the spatial distribution of mean AOD

ACPD
15, 3285–3325, 2015

for six high-value types and the associated large-scale three-dimensional atmospheric circulation structure. Each type contains a set of three different layers and differs from each other, either in terms of the position and intensity of weather systems or in the vertical allocation of the corresponding atmospheric circulations.

Firstly, the two episodes marked with the letter A in Table 1 are classified as type 1, which account for 6.7 % of all polluted days. Distribution of AOD is shown in Fig. 7a, high value appeared in Anhui province and the regional mean AOD is 0.60. The corresponding atmospheric circulations were shown in Fig. 7b–d. In detail, the sea level pressure field is characterized as the pattern before the passage of the cold front. Before the arrival of cold flow caused by the low-pressure system over northeast of China, warm air mass accumulates ahead of the front, which favors the increase of pollutants. Winds are blowing from the northwest in the both lower and middle troposphere, gradually leading cold air toward the East China. In view of the above-mentioned facts, the pollution of this type is not quite serious.

Type 2 (marked with the letter B in Table 3) is the most frequent among the six polluted types with a percentage of 40 %. It is evident that the occurrence of pollution in East China mainly requires a uniform pressure field on surface (Fig. 8). At 850 hPa level, the pattern corresponds to weak southerlies for it is controlled by the rear sector of an anticyclonic circulation. Besides, the local vorticity of type 2 is stronger than that of H1, allowing the hover of pollutants. The upper west-northwest flow is crossing the area, causing fair weather conditions. According Table 1, it seems that type 2 can last for a long time. Generally speaking, type 2 is a relatively stable and serious pollution example with a mean AOD value of 0.77.

Type 3 (marked with the letter C in Table 3) is associated with four episodes, accounting for 21.1 %. From Fig. 9a, high values center in Henan province, extending to the southeast and southwest. The circulation structure, corresponding to this type, is shown in Fig. 9b–d. On the surface, the region is governed by the periphery of a high pressure system located in Mongolia, which results low pressure gradient over the central of East China. At 500 hpa, an upper air trough cause moderate northeasterly flows,

ACPD
15, 3285–3325, 2015

the wind field in lower troposphere can be considered as anticyclonic and the wind direction is consistent with the direction of diffusion of pollutants. These conditions yield a regional average AOD value of 0.61.

Type 4 (marked with the letter D in Table 3) consists of four pollution episodes (accounts for 18.9 %), which all last for 3 to 5 days. It resembles Type 2 concerning the spatial distribution of AOD (Fig. 10a), but the contamination degree of type 4 is relatively light and mean AOD is 0.63. On the surface (Fig. 10b), the pattern is characterized by the periphery of a high barometric system, which lies over Tibetan Plateau. The lack of pressure gradient allows for formation of pollution. At 850 hPa (Fig. 10c), an anticyclone centered over the study area, results to moderate to low wind speed. In the middle troposphere, the circulation is almost zonal passing through mid-latitudes (Fig. 10d). Compared with type 2, the divergence of 850 hPa wind field and 500 hPa geopotential height gradient over East China are a bit stronger. And maybe these are why the mean AOD of type 4 is less than type 2.

Type 5 (marked with the letter E in Table 3) depicts a different pattern of pollution distribution. As shown in Fig. 11a, the main difference between these types is that, for type 5, the pollutants gather in the northeast other than the center of the studied area. Because of the relative concentration of pollution, the regional mean AOD reach 0.60 merely. Figure 11 represents the associated circulations. On the surface, East China is found in a transition zone between two weak high pressure systems, located in the western plateau and eastern ocean respectively. The southerly wind, which is controlled by the rear of weak anticyclonic circulation, dominates in the lower troposphere, while in the middle troposphere, the sparse isopleths indicate fair weather condition. This type occurred on 10 % of all polluted days in the sample.

Type 6 (marked with the letter F in Table 3) consists only one 3 day episode (accounts for 3.3 %). Very high values are found in Hunan province and average AOD of the whole area is 0.70. A surface high pressure system centered over the Yellow Sea, results to southerly flow over the East China, which also prevails in the lower troposphere. Warm-wet air flow is responsible for formation of dense inversion layer, thereby hindering the

ACPD
15, 3285–3325, 2015

vertical motion of atmosphere and resulting heavy pollution. These conditions also contribute to the northward extension of pollutants (Fig. 12a). At 500 hPa, the pattern corresponds to the southwest flow with weak geopotential height gradient. Generally, type 6 is identified as a "southerly type", transporting warm air masses from the south in all the atmospheric levels.

Similar to the pollution episodes, the results for clean episodes are detailed in the following paragraphs. The distributions of AOD and the corresponding weather maps for each clean type are shown in Figs. 13–15.

Type 7 (marked with the letter G in Table 3) is the most frequent clean type during the whole examined low-value days (accounts for 57.6 %). As shown in Fig. 13a, the maximum AOD is less than 0.6, in addition, the mean AOD for the entire region is 0.33, which represents for improved air quality by contrast with the above polluted types. According to the surface pressure pattern of type 7 (Fig. 13b), a uniform pressure field, in front of the high barometric system, affects the East China. A trough appears in the upper atmosphere, accompanied by an anticyclonic eddy in the lower troposphere, which causes moderate northwesterly winds (Fig. 13c and d). These interactions of upper and lower air circulations facilitate the removal of pollutants from the locality.

Type 8 (marked with the letter H in Table 3), which accounts for 18.2 % of all clean days, is characterized by the rear of weak high pressure system centered in the east coasts of China (Fig. 14). In accord with the pattern on surface, anticyclonic conditions are observed in 850 hPa. Therefore, it can be derived that winds are southwesterly and southeasterly, blowing away local pollutants and bringing clean air from the sea to the East China. The above conditions create a mean AOD value of 0.35.

Type 9 (marked with the letter I in Table 3) is the cleanest type with an average AOD value of 0.31. It is identified as the passage of a cold front and the associated frequency is 24.2 %. On the surface, the high pressure system over the northwest of China, along with a low pressure system centered in northeast of China, intensifies the southwards transfer of cold air masses, as it can be seen in Fig. 15. In the lower troposphere, strong northwesterly winds prevail in the region, facilitating dispersion of aerosols. The

ACPD
15, 3285–3325, 2015

dense isopleths which represents for marked geopotential height gradient, appears in middle troposphere. Generally, the advection of cold and dry air from northwest, which is shown in the whole vertical layers of atmosphere, contributes to the good air quality.

4 Summary and conclusion

In the present study, the climatological mean and interannual variation of AOD over East China (110–122° E, 28–40° N) are investigated through the statistical analysis of ten-year MODIS data (2001–2010). In consideration of weather characteristics of autumn, and slight sudden variations of pollutants emission during a short time, October is selected as typical month to study. The air qualities of total 310 days studied in this paper are represented by the satellite-based AOD and the corresponding meteorological fields are extracted from NCEP/NCAR Reanalysis dataset. In fact, the circulation patterns assessed at the three levels (surface, 850 and 500 hPa) on the episode days are identified. The main conclusions are summarized as follows.

Firstly, the daily mean AOD value ranges from 0.3 to 0.7 in large parts of the East China except for four widespread high-value centers, which are considered as possible consequences of industrial emissions or agricultural biomass burning. The fluctuation is more volatile over the region where the mean AOD is higher. It is underlined that the AOD did not show an increasing trend in October from 2001 to 2010, 2003 and 2006 are identified as the obvious clean and polluted year, respectively.

Secondly, two distinct extreme episodes (LE (21 to 24 October in 2003) and HE (28 to 31 October in 2006)) are picked to initially examine the relations between meteorological fields and air qualities. These two episodes showed similar surface pressure patterns but obvious differences between 850 hPa wind fields and 500 hPa geopotential height. Besides, the features of two sets of backward trajectories supported the distinct distributions of AOD associated with two episodes. In addition, to get a better insight into the impacts of circulation patterns on episodic events over East China, a compre-

ACPD
15, 3285–3325, 2015

hensive statistic of all 28 episodes occurred in the study period are carried out, among which there are 18 high-value episodes (90 days) and 10 low-value episodes (31 days).

Finally, according to the similarity of circulation patterns for all 28 episodes in all the three levels, the 18 pollution episodes are classified into six types, while the other 10 clean episodes are classified into three types. These types present the general circulation characteristics corresponding to different level of air quality. We briefly conclude the characteristics of nine types (six high-value types and three low-value types). Each type differs from each other, either in respect to the position and intensity of weather systems or the combination of lower and upper atmospheric circulations. Compared with the polluted types, generally, the flow of the clean types in the both middle and lower troposphere strengthened significantly. These conditions were propitious to the horizontal diffusion of air pollutants. Particularly, patterns that associated with the uniform pressure field in the East China or steady westerly flow in middle troposphere, or the control of the rear of an anticyclone are good indications of pollutions, while clean episodes occur when strong southeastward cold air advection prevails below the middle troposphere or air masses are transported from sea to the mainland.

In general, the above results have confirmed the impacts of large-scale atmospheric circulations upon aerosol distributions over East China. Since the empirical classification of weather types are convenient to correlate different circulations patterns with the different air qualities, therefore, these results are valuable as an assistance to the government decision make on balance of economic activities and pollution mitigations.

Acknowledgements. This work is supported by CAS Strategic Priority Research Program (Grant XDA05100303), Special Funds for Public Welfare of China (Grant GYHY201306077), the NSFC (Grant 41230419, 91337213 and 41205126), and the Jiangsu Provincial 2011 Program (Collaborative Innovation Center of Climate Change).

ACPD
15, 3285–3325, 2015

References

Al-Saadi, J., Szykman, J., Pierce, R. B., Kittaka, C., Neil, D., Chu, D. A., Remer, L., Gumley, L., Prins, E., Weinstock, L., Macdonald, C., Wayland, R., Dimmick, F., and Fishman, J.: Improving national air quality forecasts with satellite aerosol observations, B. Am. Meteorol. Soc., 86, 1249–1261, 2005.

Borge, R., Lumbreras, J., Vardoulakis, S., Kassomenos, P., and Rodríguez, E.: Analysis of long-range transport influences on urban PM_{10} using two-stage atmospheric trajectory clusters, Atmos. Environ., 41, 4434–4450, 2007.

Chen, B., Stein, A. F., Maldonado, P. G., Sanchez de la Campa, A. M., Gonzalez-Castanedo, Y., Castell, N., and de la Rosa, J. D.: Size distribution and concentrations of heavy metals in atmospheric aerosols originating from industrial emissions as predicted by the HYSPLIT model, Atmos. Environ., 71, 234–244, 2013.

Chen, S., Zhao, C., Qian, Y., Leung, L. R., Huang, J., Huang, Z., Bi, J., Zhang, W., Shi, J., Yang, L., Li, D., and Li, J.: Regional modeling of dust mass balance and radiative forcing over East Asia using WRF-Chem, Aeolian Res., 15, 15–30, 2014.

Chen, S. Y., Huang, J. P., Fu, Q., Ge, J. M., and Su, J.: Effects of aerosols on autumn precipitation over mid-eastern China, J. Trop. Meteorol., 27, 339–347, 2012 (in Chinese).

Chen, X. L., Fan, S. J., Li, J. N., Liu, J., Wang, A. Y., and Fong, S. K.: The typical weather characteristics of air pollution in Hong Kong area, J. Trop. Meteorol., 24, 195–199, 2008 (in Chinese).

Chen, Z. H., Cheng, S. Y., Li, J. B., Guo, X. R., Wang, W. H., and Chen, D. S.: Relationship between atmospheric pollution processes and synoptic pressure patterns in northern China, Atmos. Environ., 42, 6078–6087, 2008.

Cheng, S. Y., Chen, D. S., Li, J. B., Wang, H. Y., and Guo, X. R.: The assessment of emission-source contributions to air quality by using a coupled MM5-ARPS-CMAQ modeling system: a case study in the Beijing metropolitan region, China, Environ. Modell. Softw., 22, 1601–1616, 2007.

Chu, D. A., Kaufman, Y. J., Ichoku, C., Remer, L. A., Tanré, D., and Holben, B. N.: Validation of MODIS aerosol optical depth retrieval over land, Geophys. Res. Lett., 29, 8007, doi:10.1029/2001GL013205, 2002.

ACPD
15, 3285–3325, 2015

Csavina, J., Field, J., Félix, O., Corral-Avitia, A. Y., Eduardo Sáez, A., and Betterton, E. A.: Effect of wind speed and relative humidity on atmospheric dust concentrations in semi-arid climates, Sci. Total. Environ., 487, 82–90, 2014.

Demuzere, M., Trigo, R. M., Vila-Guerau de Arellano, J., and van Lipzig, N. P. M.: The impact of weather and atmospheric circulation on O_3 and PM_{10} levels at a rural mid-latitude site, Atmos. Chem. Phys., 9, 2695–2714, doi:10.5194/acp-9-2695-2009, 2009.

Ding, A. J., Wang, T., Zhao, M., Wang, T., and Li, Z.: Simulation of sea–land breezes and a discussion of their implications on the transport of air pollution during a multi-day ozone episode in the Pearl River Delta of China, Atmos. Environ., 38, 6737–6750, 2004.

Ding, A. J., Wang, T., Thouret, V., Cammas, J.-P., and Nédélec, P.: Tropospheric ozone climatology over Beijing: analysis of aircraft data from the MOZAIC program, Atmos. Chem. Phys., 8, 1–13, doi:10.5194/acp-8-1-2008, 2008.

Ding, A. J., Wang, T., Xue, L. K., Gao, J., Stohl, A., Lei, H. C., Jin, D. Z., Ren, Y., Wang, Z. F., Wei, X. L., Qi, Y. B., Liu, J., and Zhang, X. Q.: Transport of north China midlatitude cyclones: case study of aircraft measurements in summer 2007, J. Geophys. Res., 114, D08304, doi:10.1029/2008JD011023, 2009.

Donaldson, K., Stone, V., Seaton, A., and MacNee, W.: Ambient particle inhalation and the cardiovascular system: potential mechanisms, Environ. Health Persp., 109, 523–527, 2001.

Draxler, R. R. and Hess, G. D.: Description of the HYSPLIT_4 modeling system, NOAA Technical Memorandum ERL ARL-224, NOAA Air Resources Laboratory, Silver Spring, MD, 24 pp., available at: http://www.arl.noaa.gov/HYSPLIT_pubs.php (last access: 15 November 2014), 1997.

Flocas, H., Kelessis, A., Helmis, C., Petrakakis, M., Zoumakis, M., and Pappas, K.: Synoptic and local scale atmospheric circulation associated with air pollution episodes in an urban Mediterranean area, Theor. Appl. Climatol., 95, 265–277, 2009.

Guo, J. P., Zhang, X. Y., Wu, Y. R., Zhaxi, Y. Z., Che, H. Z., La, B., Wang, W., and Li, X. W.: Spatio-temporal variation trends of satellite-based aerosol optical depth in China during 1980–2008, Atmos. Environ., 45, 6802–6811, 2011.

Guo, Y. F., Li, D. Y., Zhou, B., Xia, J., Wu, Y., and Hu, Y. H.: Study on haze characteristics in Wuxi and its impact factors, Meteor. Mon., 39, 1314–1324, 2013 (in Chinese).

He, Q. S., Li, C. C., Geng, F. H., Lei, Y., and Li, Y. H.: Study on long-term aerosol distribution over the land of east China using MODIS data, Aerosol Air Qual. Res., 12, 304–319, 2012.

ACPD
15, 3285–3325, 2015

Janssen, N. A., Hoek, G., Simic-Lawson. M., Fischer, P., van Bree, L., ten Brink, H., Keuken, M., Atkinson, R. W., Anderson, H. R., Brunekreef, B., and Cassee, F. R.: Black carbon as an additional indicator of the adverse health effects of airborne particles compared with PM_{10} and $PM_{2.5}$, Environ. Health Persp., 119, 1691–1699, 2011.

Kan, H. and Chen, B.: Particulate air pollution in urban areas of Shanghai, China: health-based economic assessment, Sci. Total Environ., 322, 71–79, 2004.

Kassomenos, P. A.: Anatomy of the synoptic conditions occurring over southern Greece during the second half of 20 century, Part 1: winter and summer, Theor. Appl. Climatol., 75, 65–77, 2003.

Kaufman, Y. J., Tanre, D., and Boucher, O.: A satellite view of aerosols in the climate system, Nature, 419, 215–223, 2002.

Kim, S. W., Yoon, S. C., Kim, J. Y., and Kim, S. Y.: Seasonal and monthly variations of columnar aerosol optical properties over East Asia determined from multi-year MODIS, LIDAR, and AERONET sun/sky radiometer measurements, Atmos. Environ., 41, 1634–1651, 2007.

Koren, I., Altaratz, O., Remer, L. A., Feingold, G., Martins, J. V., and Heiblum, R. H.: Aerosol-induced intensification of rain from the tropics to the mid-latitudes, Nat. Geosci., 5, 118–122, doi:10.1038/NGEO1364, 2012.

Li, Z. Q., Niu, F., Fan, J. W., Liu, Y. G., Rosenfeld, D., and Ding, Y. N.: Long-term impacts of aerosols on the vertical development of clouds and precipitation, Nat. Geosci., 4, 888–894, doi:10.1038/NGEO1313, 2011.

Lin, J., Nielsen, C. P., Zhao, Y., Lei, Y. Liu, Y., and Mcelroy, M. B.: Recent changes in particulate air pollution over China observed from space and the ground: effectiveness of emission control, Environ. Sci. Technol., 44, 7771–7776, 2010.

Liu, R. C. and Li, H. Z.: The analysis of the relationship between the weather conditions and the smoke screen in Beijing, Chinese J. Atmos. Sci., 4, 69–78, 1980.

Liu, Y. K., Liu, J. F., and Tao, S.: Interannual variability of summertime aerosol optical depth over East Asia during 2000–2011: a potential influence from El Niño Southern Oscillation, Environ. Res. Lett., 8, 044034, doi:10.1088/1748-9326/8/4/044034, 2013.

Luo, Y. X., Zheng, X. B., Zhao, T. L., and Chen, J.: A climatology of aerosol optical depth over China from recent 10 years of MODIS remote sensing data, Int. J. Climatol., 34, 863–870, 2014.

ACPD
15, 3285–3325, 2015

Rosenfeld, D., Cattani, E., Melani, S., and Levizzani, V.: Considerations on daylight operation of 1.6-VERSUS 3.7-µm channel on NOAA and Metop Satellites, B. Am. Meteorol. Soc., 85, 873–881, 2004.
Rosenfeld, D., Dai, J., Yu, X., Yao, Z. Y., Xu, X. H., Yang, X., and Du, C. L.: Inverse relations between amounts of air pollution and orographic precipitation, Science, 315, 1396–1398, 2007.
Russo, A., Trigo, R. M., Martins, H., and Mendes, M. T.: NO_2, PM_{10} and O_3 urban concentrations and its association with circulation weather types in Portugal, Atmos. Environ., 89, 768–785, 2014.
Saavedra, S., Rodríguez, A., Taboada, J. J., Souto, J. A., and Casares, J. J.: Synoptic patterns and air mass transport during ozone episodes in northwestern Iberia, Sci. Total Environ., 441, 97–110, 2012.
Shahgedanova, M., Burt, T. P., and Davies, T. D.: Synoptic climatology of air pollution in Moscow, Theor. Appl. Climatol., 61, 85–102, 1998.
Tanner, P. A. and Law, P. T.: Effects of synoptic weather systems upon the air quality in an Asian megacity, Water Air Soil Poll., 136, 105–124, 2002.
Twomey, S.: The influence of pollution on the shortwave albedo of clouds, J. Atmos. Sci., 34, 1149–1152, 1977.
Wang, J., Li, J. L., and Zhang, Y. H.: Weather situation classification and its feature in severe air pollution days in winter in Urumqi, J. Meteor. Environ., 29, 28–32, 2013 (in Chinese).
Wang, S. X. and Zhang, C. Y.: Spatial and temporal distribution of air pollutant emissions from open burning of crop residues in China, China Science Paper Online, 3, 329–333, 2008 (in Chinese).
Wang, X. Q., Qi, Y. B., Wang, Z. F., Guo, H., and Yu, T.: The influence of synoptic pattern on PM_{10} heavy air pollution in Beijing, Climatic Environ. Res., 12, 81–86, 2007 (in Chinese).
Wu, J., Guo, J., and Zhao, D. M.: Characteristics of aerosol transport and distribution in East Asia, Atmos. Res., 132, 185–198, 2013.
Xu, W. Y., Zhao, C. S., Ran, L., Deng, Z. Z., Liu, P. F., Ma, N., Lin, W. L., Xu, X. B., Yan, P., He, X., Yu, J., Liang, W. D., and Chen, L. L.: Characteristics of pollutants and their correlation to meteorological conditions at a suburban site in the North China Plain, Atmos. Chem. Phys., 11, 4353–4369, doi:10.5194/acp-11-4353-2011, 2011.

ACPD
15, 3285–3325, 2015

Zhang, L., Liao, H., and Li, J. P.: Impacts of Asian summer monsoon on seasonal and interannual variations of aerosols over eastern China, J. Geophys. Res., 115, D00K05, doi:10.1029/2009JD012299, 2010.

Zhao, C., Wang, Y., Yang, Q., Fu, R., Cunnold, D., and Choi, Y.: Impact of East Asian summer monsoon on the air quality over China: view from space, J. Geophys. Res., 115, D09301, doi:10.1029/2009JD012745, 2010.

Zhao, C., Liu, X., and Leung, L. R.: Impact of the Desert dust on the summer monsoon system over Southwestern North America, Atmos. Chem. Phys., 12, 3717–3731, 2012, http://www.atmos-chem-phys.net/12/3717/2012/.

Zhao, C., Leung, L. R., Easter, R., Hand, J., and Avise, J.: Characterization of speciated aerosol direct radiative forcing over California, J. Geophys. Res., 118, 2372–2388, doi:10.1029/2012JD018364, 2013a.

Zhao, C., Liu, X., Qian, Y., Lin, G., McFarlane, S., Yoon, J., Wang, H., Hou, Z., Yang, B., Ma, P., Yan, H., and Bao, J.: Sensitivity of Radiative Fluxes at Top of Atmosphere to Cloud-Microphysics and Aerosol Parameters in the Community Atmosphere Model (CAM5), Atmos. Chem. Phys., 13, 10969–10987, 2013b, http://www.atmos-chem-phys.net/13/10969/2013/.

Zhao, C. S., Tie, X. X., and Lin, Y. P.: A possible positive feedback of reduction of precipitation and increase in aerosols over eastern central China, Geophys. Res. Lett., 33, L11814, doi:10.1029/2006GL025959, 2006a.

Zhao, C. S., Tie, X. X., Brasseur, G., Noone, K. J., Nakajima, T., Zhang, Q., Zhang, R. Y., Huang, M. Y., Duan, Y., Li, G. L., and Ishizaka, Y.: Aircraft measurements of cloud droplet spectral dispersion and implications for indirect aerosol radiative forcing, Geophys. Res. Lett., 33, L16809, doi:10.1029/2006GL026653, 2006b.

Ziomas, I., Melas, D., Zerefos, C., Bais, A., and Paliatsos, A.: Forecasting peak pollutant levels from meteorological variables, Atmos. Environ., 29, 3703–3711, 1995.

Zortie, E. and von Storch, H.: The analog method as a simple statistical downscaling technique: comparison with more complicated methods, J. Climate., 12, 2474–2489, 1999.

ACPD
15, 3285–3325, 2015

Table 1. Short description for the observed meteorological fields features for 18 pollution episodes. (The rows in the table with same capital letters in the parentheses indicate those episodes are affected by the similar circulation patterns in all the three atmospheric levels.)

Episodes	Year (Date)	Surface	850 hPa	500 hPa
1 (A)	2002 (01–04)	Before the passage of a cold front	strong cold wind blow to south	NW flow
2 (B)	2002 (08–16)	Uniform pressure field	the rear of anticyclone	W–NW flow
3 (C)	2002 (24–26)	Periphery of the high pressure system centered in the Mongolia	the foreside of anticyclone	NW flow (behind the trough)
4 (C)	2004 (07–13)	Periphery of the high pressure system centered in the Mongolia	the foreside of anticyclone	NW flow (behind the trough)
5 (D)	2004 (18–22)	Periphery of the high pressure system centered in the TP	anticyclonic circulation	W flow
6 (F)	2004 (27–29)	The rear of high pressure system	South wind	SW flow
7 (D)	2005 (16–18)	Periphery of the high pressure system centered in the TP	anticyclonic circulation	Shallow trough
8 (E)	2005 (23–26)	A transition zone between two weak high pressure systems	the rear of anticyclone	W–NW flow
9 (B)	2006 (04–15)	Uniform pressure field	the rear of anticyclone	W–NW flow
10 (D)	2006 (28–31)	Periphery of the high pressure system centered in the TP	the foreside of anticyclone	Shallow trough
11 (B)	2007 (16–25)	Uniform pressure field	anticyclonic circulation	W–NW flow
12 (B)	2008 (01–03)	Uniform pressure field	the rear of anticyclone	NW flow
13 (E)	2008 (13–17)	A transition zone between two weak high pressure systems	the rear of anticyclone	W–NW flow
14 (C)	2009 (02–06)	Periphery of the high pressure system centered in the Mongolia	the foreside of anticyclone	NW flow (behind the trough)
15 (A)	2009 (15–16)	Before the passage of a cold front	strong cold flow toward south	NW flow
16 (D)	2009 (21–25)	Periphery of the high pressure system centered in the TP	anticyclonic circulation	W flow
17 (B)	2010 (16–17)	Periphery of the high pressure system centered in the Mongolia	the rear of anticyclone	NW flow
18 (C)	2010 (28–31)	Periphery of the high pressure system centered in the Mongolia	the foreside of anticyclone	NW flow (behind the trough)

ACPD
15, 3285–3325, 2015

Table 2. As in Table 1, but for 10 pollution episodes.

Episodes	Year (Date)	Surface	850 hPa	500 hPa
1 (G)	2001 (10–11)	Periphery of the high pressure system	anticyclonic circulation	NW flow (behind the trough)
2 (H)	2001 (29–30)	the rear of high pressure system	anticyclonic circulation	W flow
3 (G)	2003 (15–18)	Periphery of the high pressure system	the foreside of anticyclone, strong wind	NW flow
4 (G)	2003 (21–24)	Periphery of the high pressure system	the foreside of anticyclone, strong wind	NW flow
5 (G)	2003 (27–29)	Periphery of the high pressure system	the foreside of anticyclone, strong wind	NW flow
6 (G)	2004 (02–04)	Uniform pressure field	anticyclonic circulation	NW flow (behind the trough)
7 (H)	2005 (08–10)	the rear of high pressure system	anticyclonic circulation	W flow
8 (I)	2008 (23–26)	The passage of cold front	strong cold wind	NW flow
9 (I)	2009 (17–20)	The passage of cold front	strong cold wind	NW flow
10 (G)	2010 (03–04)	Periphery of the high pressure system	anticyclonic circulation, strong wind	NW flow (behind the trough)

ACPD
15, 3285–3325, 2015

Table 3. Short description of the statistical results for six pollution episodes and three clean episodes. Note: the capital letters in the parentheses of each row corresponds to that of Tables 1 and 2.

Episodes	Type	AOD	Surface	850 hPa	500 hPa	Percentage (%)
High AOD	1 (A)	0.60	Before the passage of a cold front	strong cold flow toward south	NW flow	6.7
	2 (B)	0.78	Uniform pressure field	the rear of anticyclone	W–NW flow	40.0
	3 (C)	0.61	Periphery of the high pressure system centered in the Mongolia	the foreside of anticyclone	NW flow (behind the trough)	21.1
	4 (D)	0.63	Periphery of the high pressure system centered in the TP	anticyclonic circulation	W flow	18.9
	5 (E)	0.60	A transition zone between two weak high pressure systems	the rear of anticyclone	W–NW flow	10
	6 (F)	0.70	The rear of high pressure system	the rear of anticyclone	SW flow	3.3
Low AOD	7 (G)	0.33	Periphery of the high pressure system	the foreside of anticyclone, strong wind	NW flow (behind the trough)	57.6
	8 (H)	0.35	the rear of high pressure system	anticyclonic circulation	W flow	18.2
	9 (I)	0.31	The passage of cold front	strong cold wind	NW flow	24.2

ACPD
15, 3285–3325, 2015

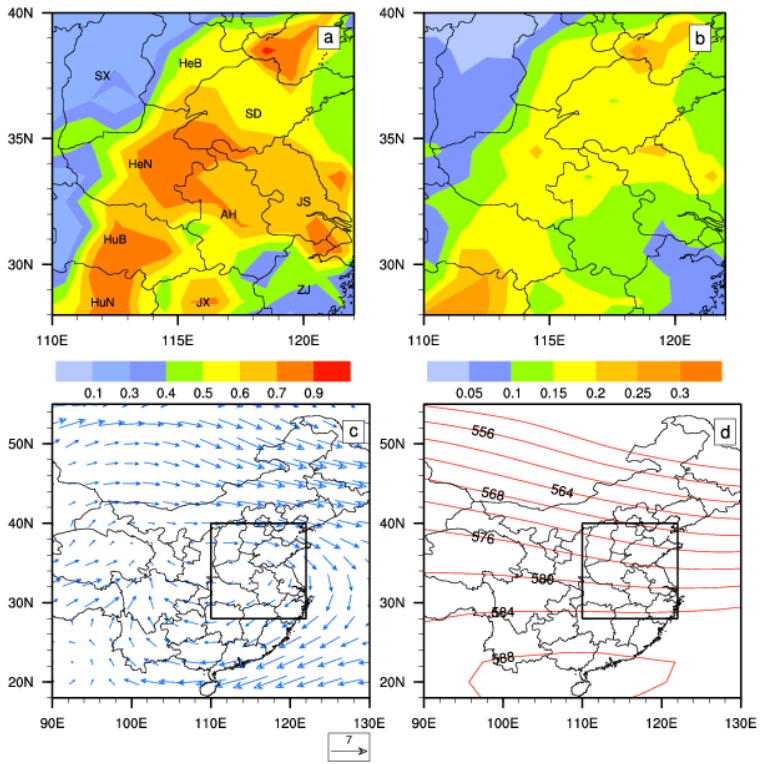

Figure 1. The mean distribution of **(a)** aerosol optical depth (AOD); **(b)** SD of AOD; **(c)** 850 hPa winds field; **(d)** 500 hPa geopotential height field in October for the period from 2001 to 2010. (Black letters on **(a)** indicate the different provinces. SX: Shanxi; SD: Shandong; HeB: Hebei; HeN: Henan; HuB: Hubei; HuN: Hunan; AH: Anhui; JX: Jiangxi; JS: Jiangsu; ZJ: Zhejiang.) Note: black rectangular region in **(c)** and **(d)** represents the East China (110–122° E, 28–40° N).

ACPD
15, 3285–3325, 2015

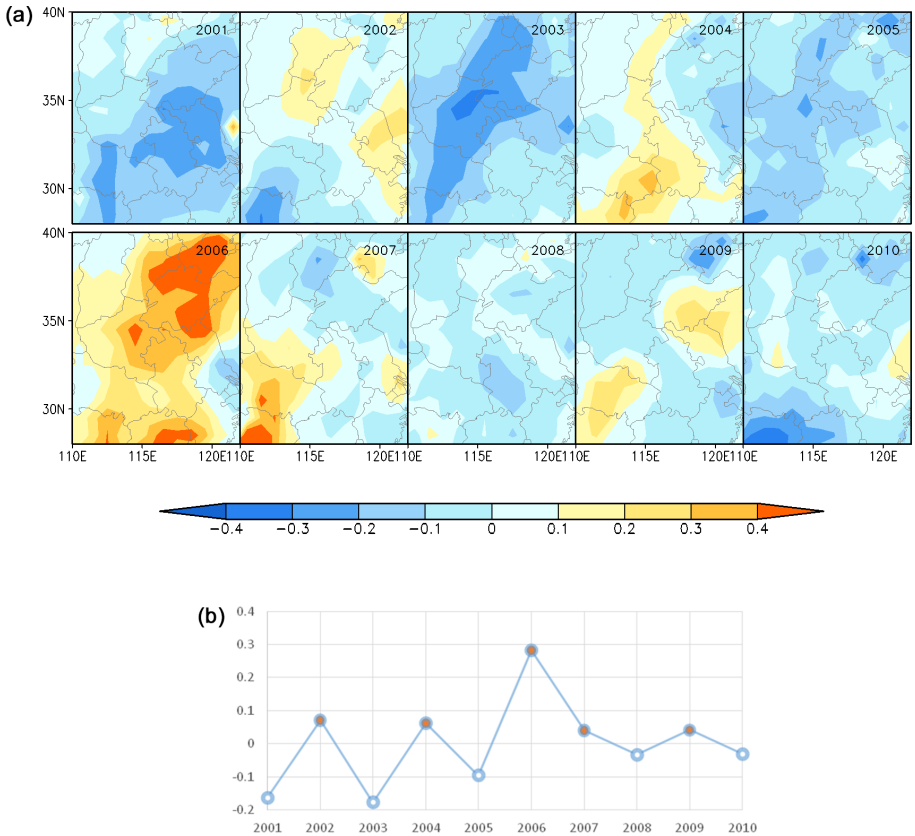

Figure 2. (a) The distribution of AOD anomaly over East China in October for 2001–2010. **(b)** Interannual variability of AOD anomaly which is averaged over the region shown in **(a)**.

ACPD
15, 3285–3325, 2015

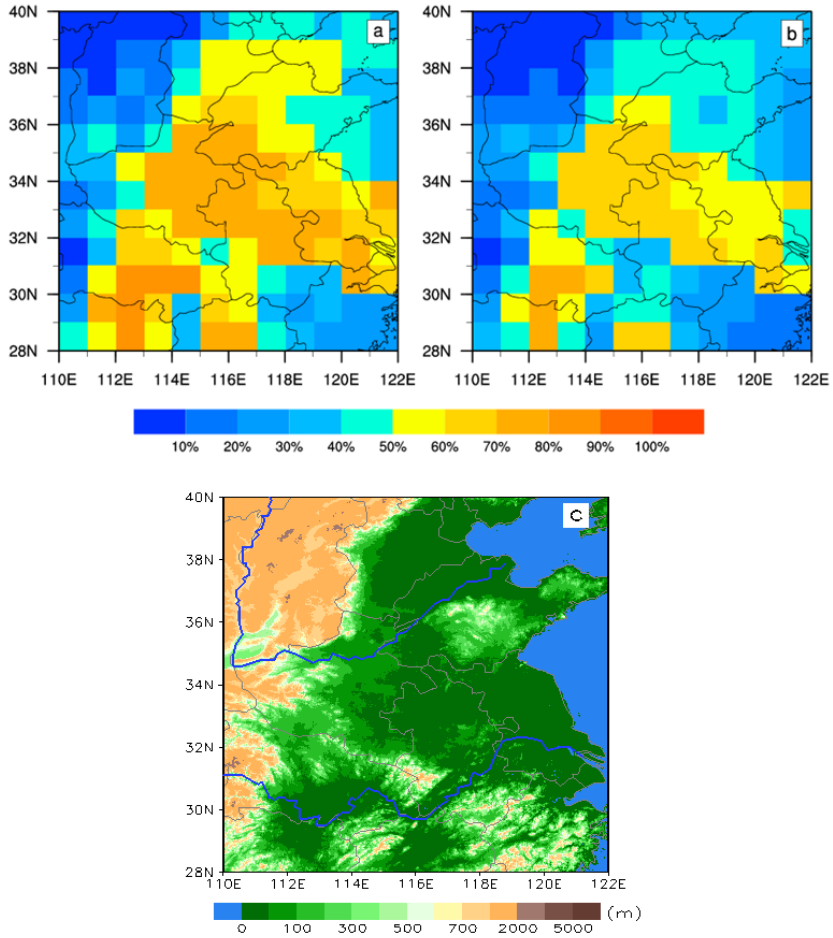

Figure 3. Frequency distribution of **(a)** AOD > 0.5 and **(b)** AOD > 0.6 in October calculated from 2001 to 2010, **(c)** the topography of East China.

ACPD
15, 3285–3325, 2015

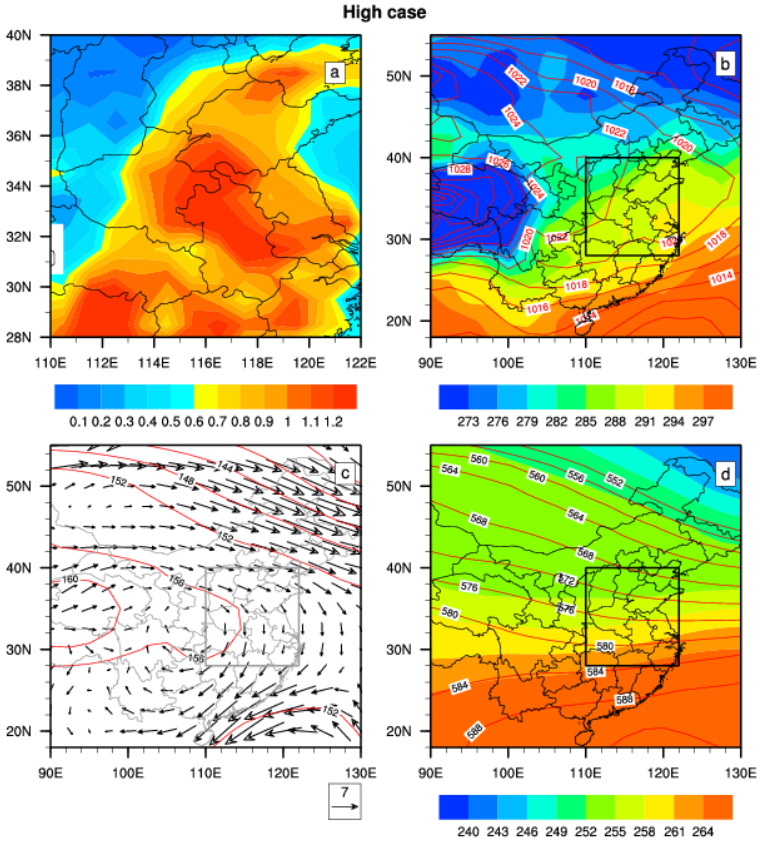

Figure 4. One typical polluted episode (28–31 October 2006). **(a)** The distribution of AOD over East China **(b)** sea level pressure (red line) and temperature (color shades) fields; **(c)** 850 hPa wind and geopotential height (red line) fields; **(d)** 500 hPa temperature (color shades) and geopotential height (red line) fields;. Note: black rectangular region represents the East China (110–122° E, 28–40° N).

ACPD
15, 3285–3325, 2015

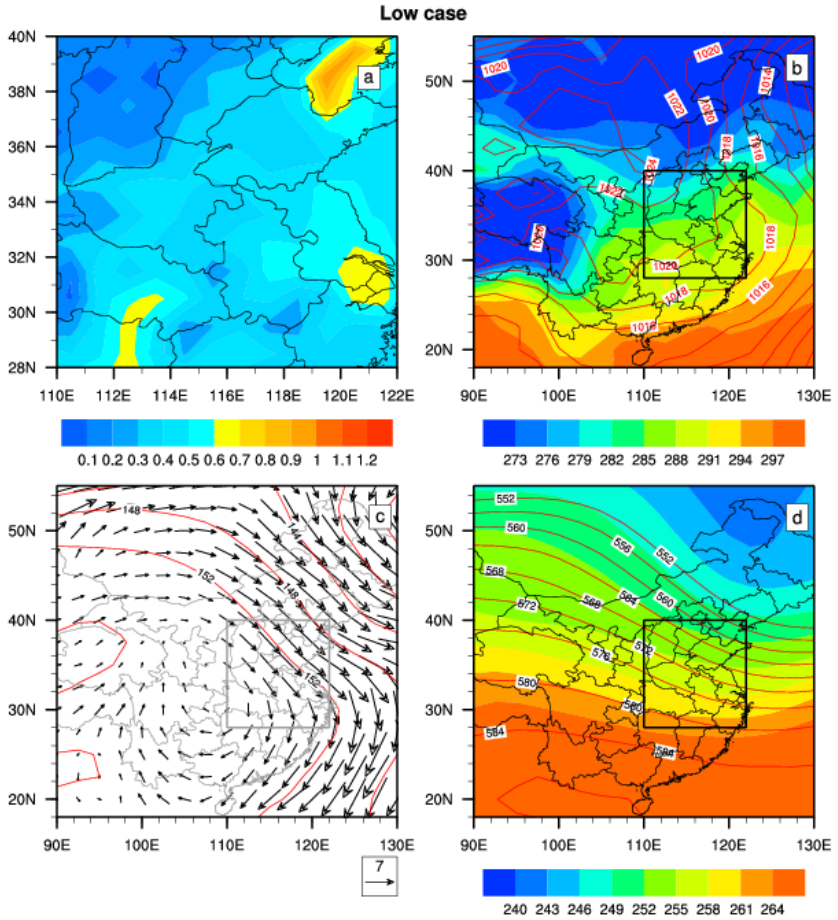

Figure 5. As in Fig. 4, but for the clean episode (21–24 October 2003).

ACPD
15, 3285–3325, 2015

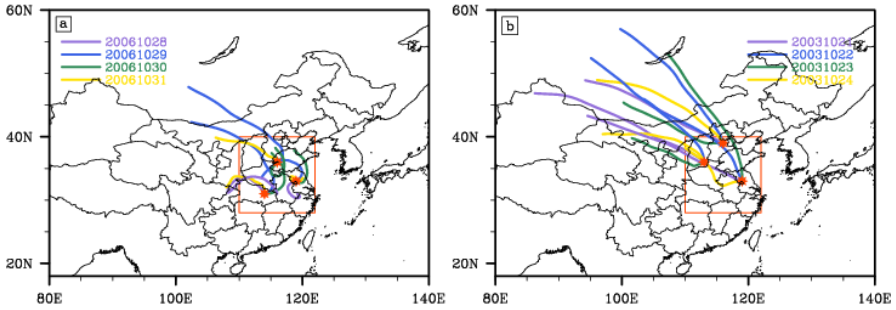

Figure 6. The 48 h backward trajectories for two episodes over East China (red box), three red star represent three ending points: **(a)** pollution episode, at 31° N, 114° E; 33° N, 119° E; 36° N, 116° E. **(b)** Clean episode, at 33° N, 119° E; 36° N, 113° E; 39° N, 116° E.

ACPD
15, 3285–3325, 2015

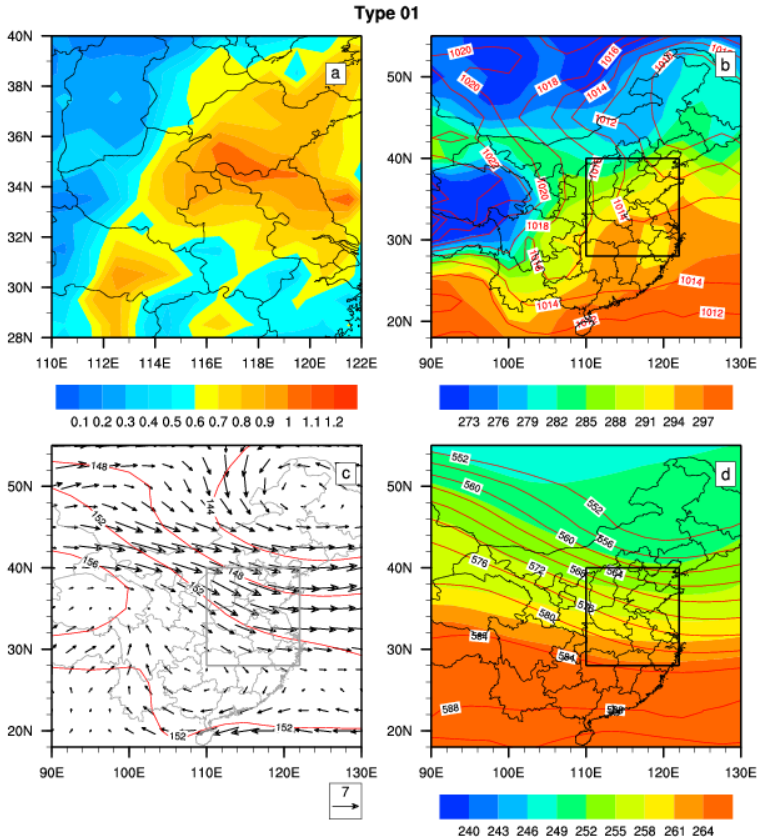

Figure 7. Type 1 (polluted): **(a)** the distribution of AOD over East China **(b)** sea level pressure (red line) and temperature (color shades) fields; **(c)** 850 hPa wind field and geopotential height (red line) fields; **(d)** 500 hPa temperature (color shades) and geopotential height (red line) fields. Note: black rectangular region represents the East China (110–122° E, 28–40° N).

ACPD
15, 3285–3325, 2015

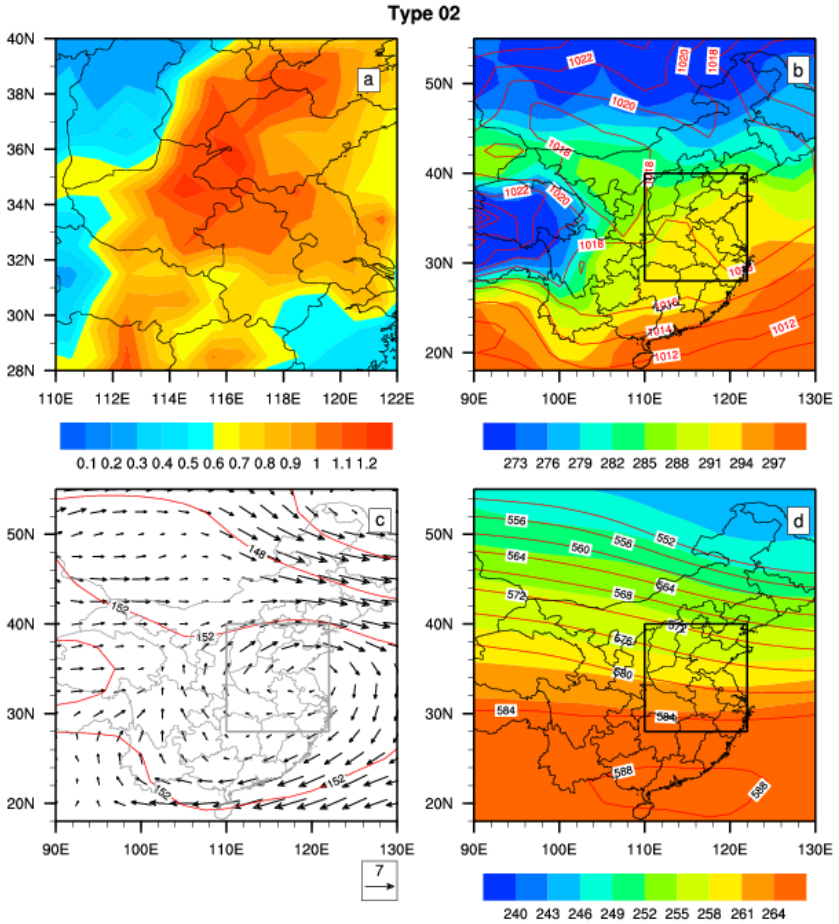

Figure 8. As in Fig. 7, but for the type 2 (polluted).

ACPD
15, 3285–3325, 2015

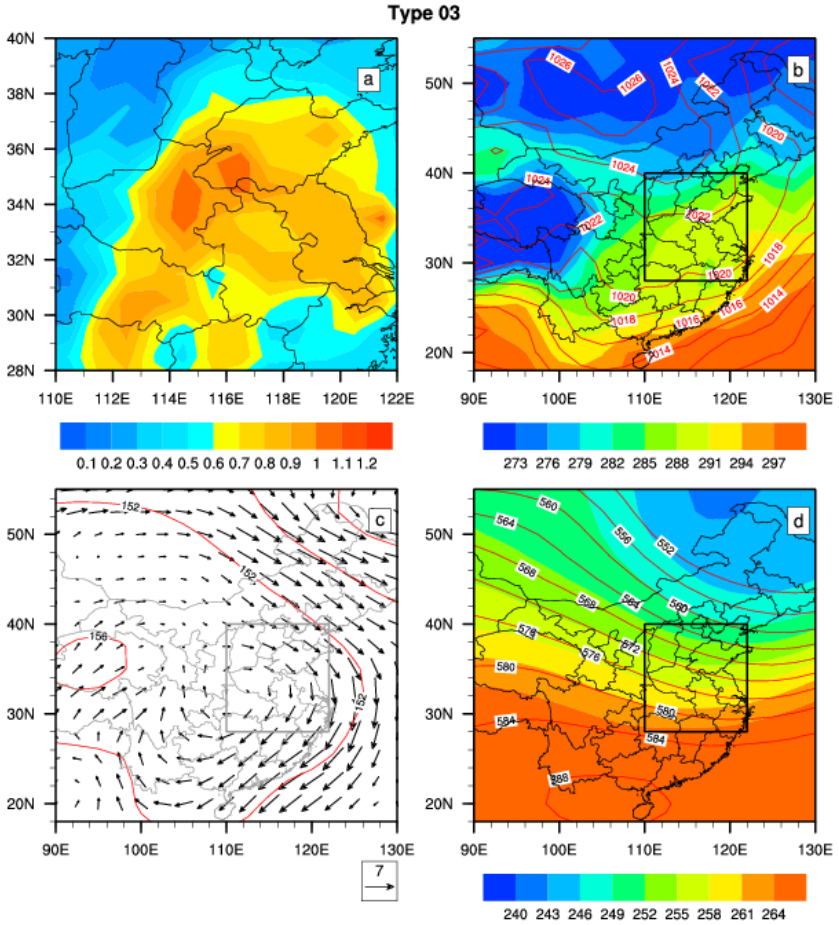

Figure 9. As in Fig. 7, but for the type 3 (polluted).

ACPD
15, 3285–3325, 2015

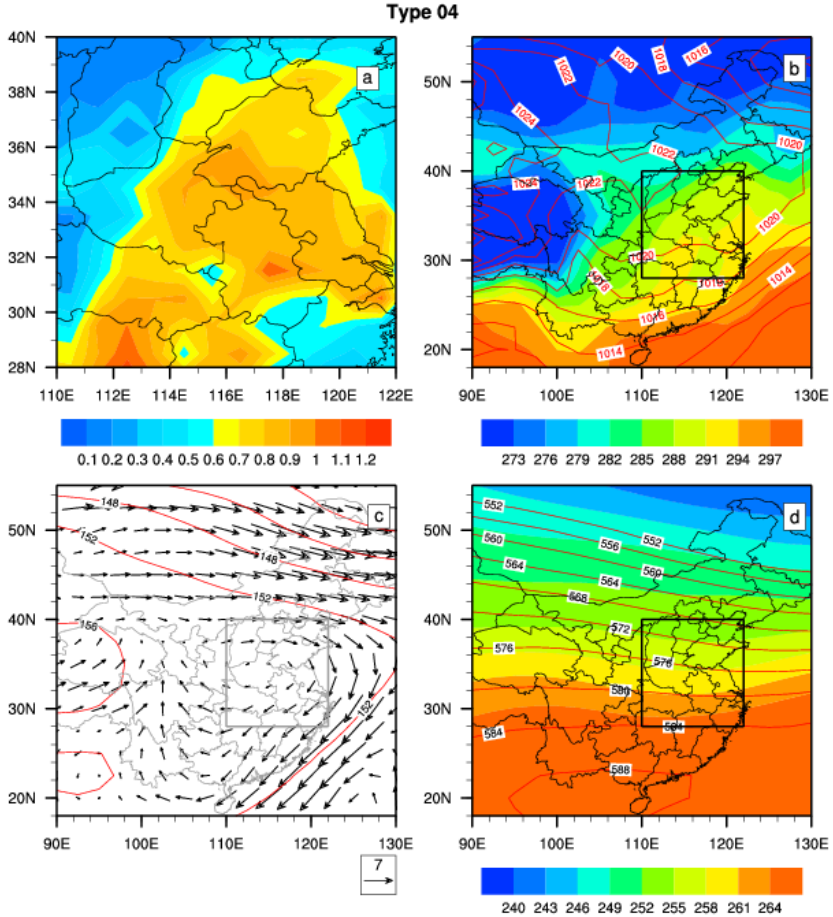

Figure 10. As in Fig. 7, but for the type 4 (polluted).

ACPD
15, 3285–3325, 2015

Impacts of atmospheric circulations on aerosol distributions

X.-Y. Zheng et al.

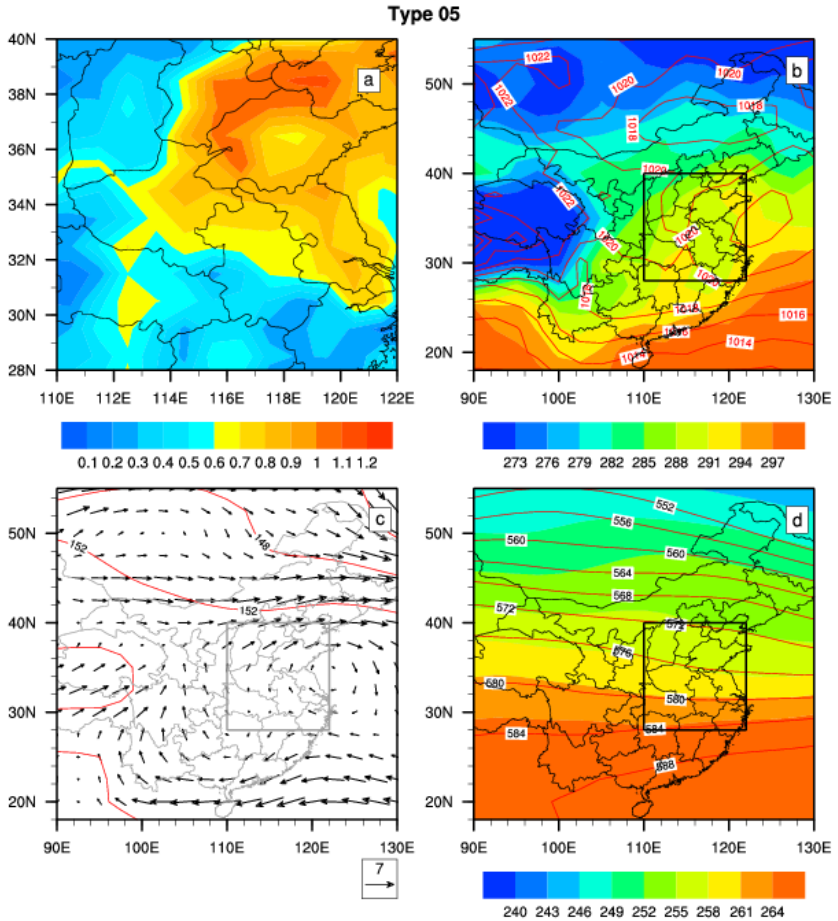

Figure 11. As in Fig. 7, but for the type 5 (polluted).

ACPD
15, 3285–3325, 2015

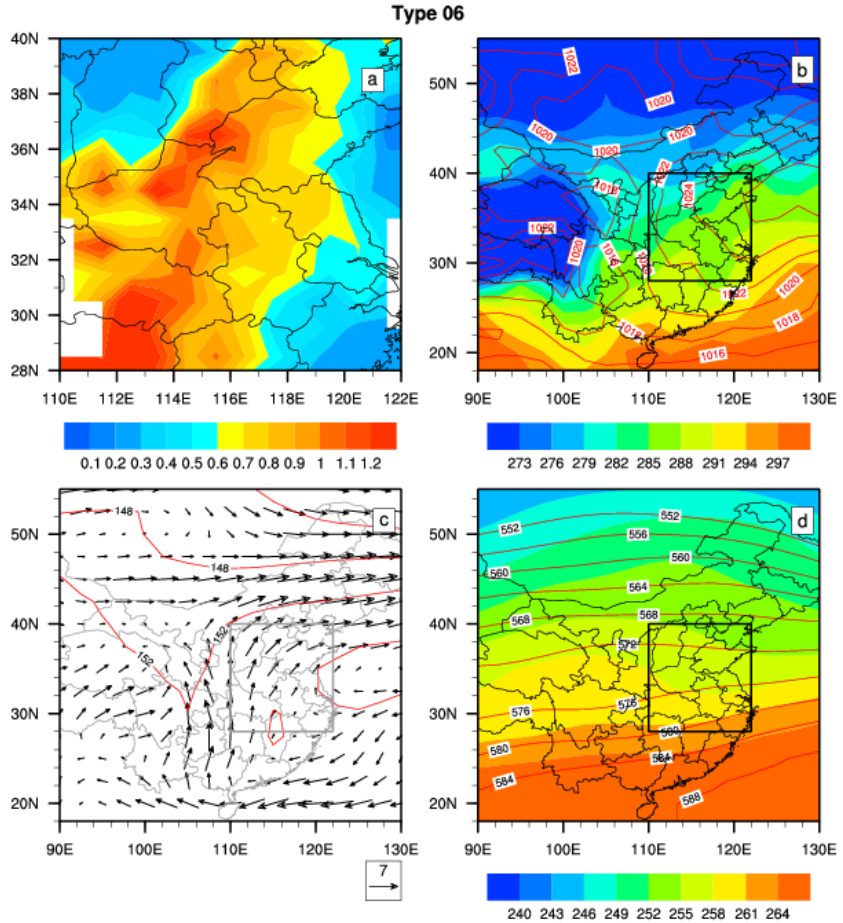

Figure 12. As in Fig. 7, but for the type 6 (polluted).

ACPD
15, 3285–3325, 2015

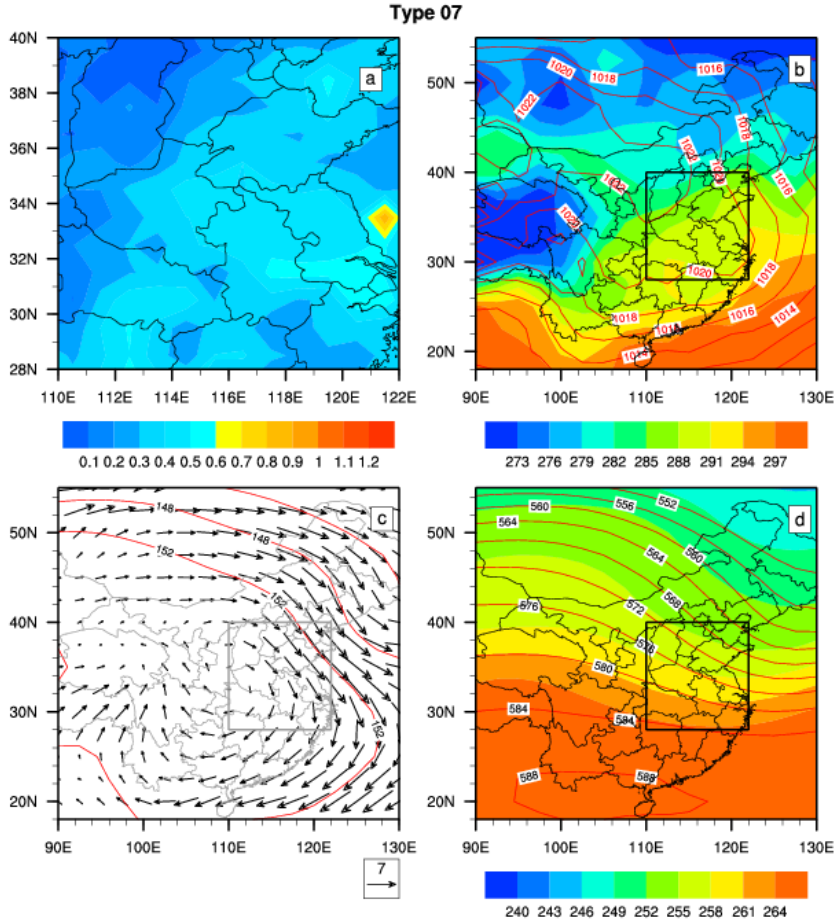

Figure 13. As in Fig. 7, but for the type 7 (clean).

ACPD
15, 3285–3325, 2015

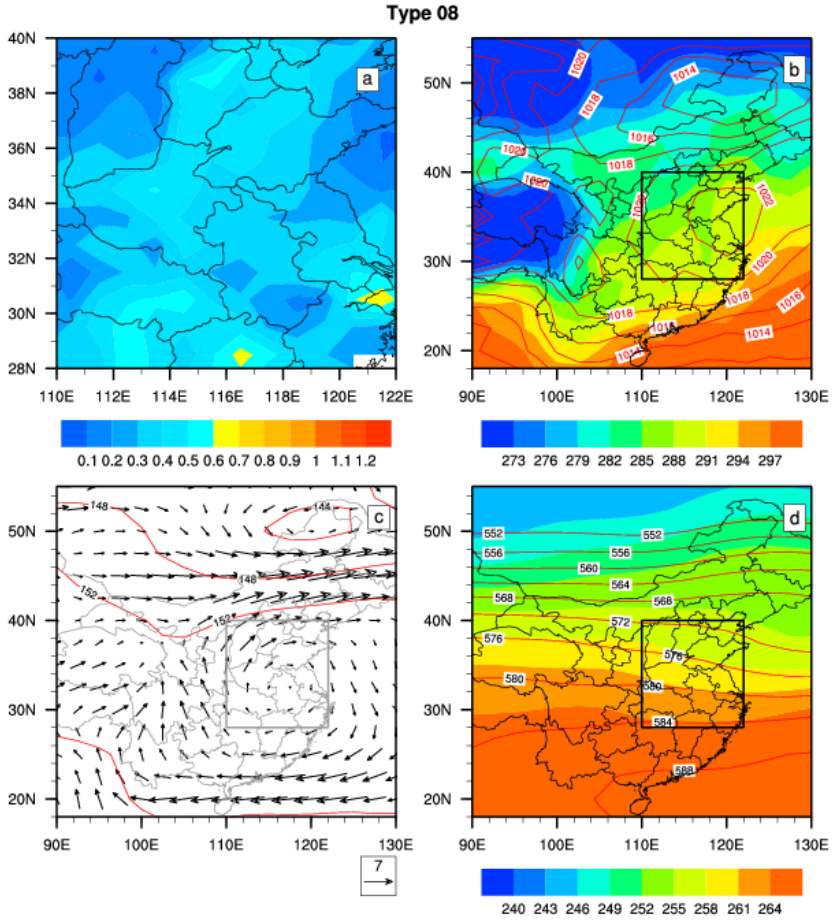

Figure 14. As in Fig. 7, but for the type 8 (clean).

ACPD
15, 3285–3325, 2015

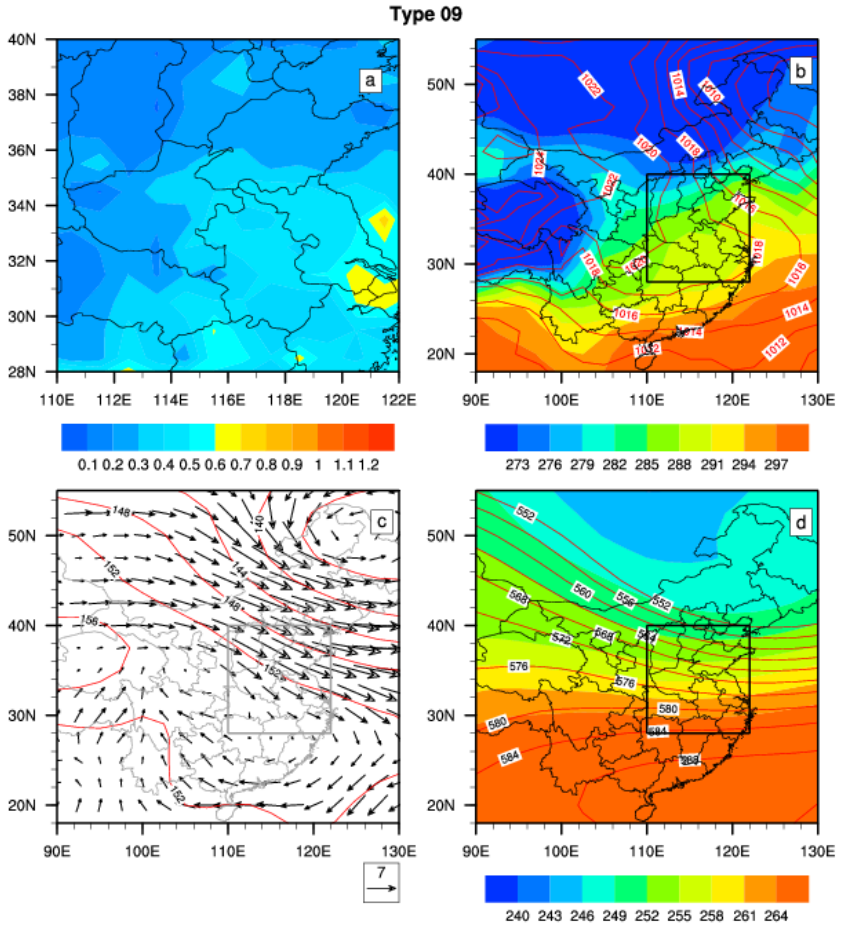

Figure 15. As in Fig. 7, but for the type 9 (clean).

ACPD
15, 3285–3325, 2015